Nano Research 2018, 11(2): 676–685
https://doi.org/10.1007/s12274-017-1674-4
Research Article

ISSN 1998-0124
CN 11-5974/O4

Gold nanoshells: Contrast agents for cell imaging by cardiovascular optical coherence tomography

Jie Hu[1,§], Francisco Sanz-Rodríguez[1,2,3,§], Fernando Rivero[4], Emma Martín Rodríguez[1,2] (✉), Río Aguilar Torres[4], Dirk H. Ortgies[1,2], José García Solé[1], Fernando Alfonso[4], and Daniel Jaque[1,2]

[1] *Fluorescence Imaging Group, Departamento de Física de Materiales, Instituto Nicolás Cabrera, Facultad de Ciencias, Universidad Autónoma de Madrid, Madrid 28049, Spain*
[2] *Instituto Ramón y Cajal de Investigación Sanitaria, Hospital Ramón y Cajal, Madrid 28034, Spain*
[3] *Departamento de Biología, Universidad Autónoma de Madrid, Madrid 28049, Spain*
[4] *Cardiology Department, Hospital Universitario de la Princesa, IIS-IP, Universidad Autónoma de Madrid, Madrid 28006, Spain*
[§] *Jie Hu and Francisco Sanz-Rodríguez contributed equally to the work.*

Received: 25 January 2017
Revised: 9 May 2017
Accepted: 10 May 2017

KEYWORDS

optical coherence tomography (OCT)
intravascular imaging,
gold nanoparticles,
three-dimensional (3D) imaging

ABSTRACT

Optical coherence tomography (OCT) has gained considerable attention in interventional cardiovascular medicine and is currently used in clinical settings to assess atherosclerotic lesions and to optimize stent placement. Artery imaging at the cellular level constitutes the first step towards cardiovascular molecular imaging, which represents a major advance in the development of personalized noninvasive therapies. In this work, we demonstrate that cardiovascular OCT can be used to detect individual cells suspended in biocompatible fluids. Importantly, the combination of this catheter-based clinical technique with gold nanoshells (GNSs) as intracellular contrast agents led to a substantial enhancement in the backscattered signal produced by individual cells. This cellular contrast enhancement was attributed to the large backscattering cross-section of GNSs at the OCT laser wavelength (1,300 nm). A simple intensity analysis of OCT cross-sectional images of suspended cells makes it possible to identify the sub-population of living cells that successfully incorporated GNSs. The generalizability of this method was demonstrated using two different cell lines (HeLa and Jurkat cells). This work provides novel insights into cardiovascular molecular imaging using specifically modified GNSs.

1 Introduction

Optical coherence tomography (OCT) is a low-coherence interferometric imaging technique that is increasingly employed for a wide variety of medical purposes [1–3]. This relatively new minimally invasive optical technique is based on the detection of the backscattered infrared signal emitted by a broadband laser diode at tissue interfaces [4]. Interference between forward and backscattered radiation allows for in-depth

---

Address correspondence to emma.martin@uam.es

TSINGHUA UNIVERSITY PRESS Springer

localization of tissue boundaries according to the associated refractive index singularity. This simple approach allows for fast, high-quality, and high-resolution three-dimensional tissue imaging. OCT has a reasonably good penetration depth (a few mm), while maintaining a high spatial resolution, which could be as good as 1 μm, depending on the OCT modality [5, 6]. Indeed, this resolution is much better than that of other imaging technologies, such as computer X-ray tomography, nuclear magnetic resonance imaging, proton emission tomography, and ultrasound imaging. OCT offers a spatial resolution that is intermediate between those of optical microscopy and whole body imaging. It has mostly been used in ophthalmology, but also in gastroenterology, dermatology, and dentistry [1]. Owing to the simultaneous development of new laser sources in the near infrared and the miniaturization of frequency-domain Fourier analyzers to a micro-photonic scale, OCT can currently be employed in endoscopic modalities and accordingly has gained considerable attention in clinical cardiovascular imaging [7]. Cardiovascular optical coherence tomography (CV-OCT) imaging is now used as a noninvasive technique for the *in vivo* identification and assessment of unstable plaques as well as for the guidance of interventional procedures, such as atherectomies and stent placements [8–12]. The possibility of adding molecular contrast to available CV-OCT systems opens a new avenue to extend the impact of OCT to cardiovascular clinical applications, as it would enable functional biomolecular imaging together with available morphological imaging. Indeed, CV-OCT with molecular contrast would enable site-specific cardiovascular imaging and therefore would allow for the early detection and localization of atherosclerotic lesions, which are not possible using current CV-OCT imaging techniques. Thus, this cardiovascular molecular imaging modality would contribute substantially to the future development of personalized medicine for cardiovascular diseases.

A common strategy to improve OCT contrast at the molecular level involves the use of nanoparticles (NPs) that enhance OCT contrast and, at the same time, can be properly functionalized with antibodies to target specific proteins overexpressed by the tissue/cells to be detected [13]. In this respect, gold nanoparticles (GNPs) of different geometries and sizes have been successfully applied as OCT contrast enhancers [14–20]. GNPs are particularly suitable for OCT contrast enhancement as their extinction spectra can be precisely tuned over a broad spectral range solely by controlling their size and geometry. In addition, the gold surface of GNPs is particularly suitable for functionalization with specific targeting ligands and therefore provides the opportunity for molecular targeting [20]. Owing to these properties, GNPs have already been deployed as contrast agents in different OCT modalities, particularly for tissue imaging [21–23]. Moreover, gold is considered an inert, nontoxic, and biocompatible noble metal. In principle, GNPs are considered nontoxic, although some concerns have been raised, especially related to the long-term effect of gold accumulation in the organism or cellular modifications [24].

When using GNPs for molecular imaging in CV-OCT systems, the operational wavelength has to be considered. CV-OCT is based on a frequency-domain OCT catheter-guided wire that emits infrared laser light ranging from about 1,250 to 1,350 nm and at the same time records the backscattered light, while simultaneously rotating and pulling back the catheter inside the artery. Consequently, contrast agents used for molecular imaging by CV-OCT should present a large backscattering cross-section at 1,300 nm, they should be detectable in biocompatible fluids, and, finally, they should be observable even under dynamic flow conditions. Very recently, it was reported that a variety of commercial GNPs, including gold nanorods and gold nanoshells (GNSs), with plasmon resonances in the proximity of 1,300 nm, could act as efficient CV-OCT enhancers when suspended in biomedical fluids [18]. In particular, GNSs consisting of a dielectric silica core of about 200 nm and an ultrathin metal shell of about 15 nm, result in the largest CV-OCT contrast enhancement based on their superior backscattering cross-section (0.7×10^{-10} cm^2) at the CV-OCT wavelength [18]. As a result, GNSs dispersed in physiological solutions could be individually observed by CV-OCT, even under dynamic flow conditions. Despite these promising features, the potential use of GNSs for the selective enhancement of live cell imaging by CV-OCT has not been explored, though it would constitute the first step towards the use of CV-OCT for molecular imaging.

In this study, we systematically investigated CV-OCT contrast in living cells and its enhancement by passive incubation with GNSs. Experiments were conducted in two different cell lines, adherent cells (HeLa), and nonadherent cells (Jurkat). These two cell models are comparable to two human cell types; human endothelial cells correspond to the adherent cells and leukocytes to the nonadherent cells. Jurkat cells are an optimal *in vitro* model, since they are T lymphocytes, which are found in the bloodstream. Intensity analysis of CV-OCT was used to discriminate the population of living cells in which efficient incorporation of GNS was achieved and to determine the relationship between the incorporation efficiency and incubation parameters. Results extracted from CV-OCT images of cell dispersions were compared to images obtained by transmission electron microscopy (TEM) and dark field microscopy (DFM), in order to unequivocally correlate the contrast enhancement observed in the CV-OCT images with the incorporation of GNS in living cells. Future implications of the results for the application of CV-OCT to intracoronary molecular imaging are also discussed.

2 Experimental

2.1 Clinical OCT system

A commercially available CV-OCT imaging system (Dragon-Fly^{TM} OPTIS^{TM}; St. Jude Medical, St. Paul, MN, USA) available at the Interventional Cardiology Unit of the Hospital Universitario La Princesa (Madrid, Spain) was used. Figure 1(a) shows a schematic diagram of this CV-OCT system. In the set-up, a compact 1,320 nm wavelength laser was coupled to a single-mode fiber incorporated into a catheter with a 0.9 mm diameter. The single-mode fiber inside the catheter was optically coupled to a frequency-domain Michelson interferometer with different lenses and a rotating micro-reflector. This reflector deviates the laser beam 90° with respect to the fiber. The whole optical system was inserted in a tube (3-mm inner diameter) into which solutions of living cells dispersed in phosphate-buffered saline (PBS) were injected for imaging. The optical system constituted by the optical fiber and deflecting mirror rotates at a constant angular frequency by recording the 1,320 nm backscattered light generated by the suspended cells. This backscattered light was analyzed using a frequency-domain Michelson interferometer in order to produce cross-sectional OCT signals of the tubing containing the cell suspension. The axial resolution of our CV-OCT system was approximately 15 μm, with a penetration length larger than 3 mm. The catheter was also coupled to a motorized stage that allows for pullback of 5 cm inside the tubing. Simultaneous recording of cross-sectional images during the pullback procedure allowed for the three-dimensional imaging of cell suspensions.

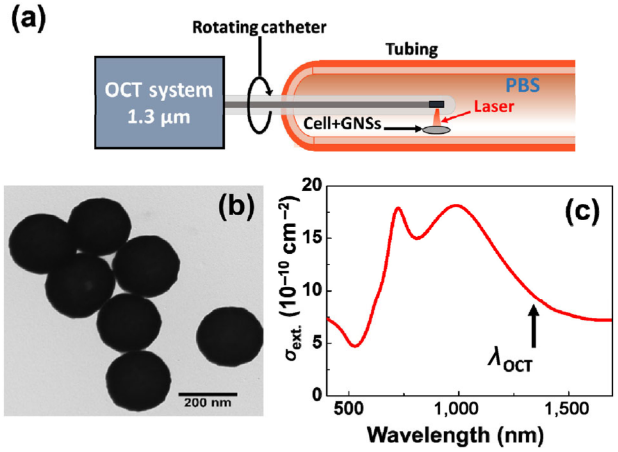

Figure 1 (a) Schematic representation of the experimental set-up employed in this work for CV-OCT imaging of suspended cells in PBS. (b) TEM image of the GNSs used during this work, with an average diameter of 198 nm. (c) Extinction spectrum of an aqueous colloidal solution of GNSs. The concentration of GNSs in the solution was set to 2.5 μg/mL. The arrow indicates the wavelength peak of the CV-OCT laser system.

2.2 Gold nanoshells

The gold nanoshells used in this work were purchased from nanoComposix Inc. (San Diego, CA, USA). Figure 1(b) shows a representative TEM image of the nanoparticles: They exhibited a total average diameter of 230 ± 10 nm with a silica core of 200 ± 10 nm. The extinction spectrum of a colloidal suspension of GNSs is shown in Fig. 1(c). Due to the contribution of multipolar plasmonic excitations, GNSs showed a broad extinction band extending from the visible to the infrared. The extinction cross-section at the CV-OCT laser wavelength (1,320 nm) was 7.6×10^{-10} cm^2. Previous estimates of the scattering and backscattering cross-sections at the CV-OCT peak wavelength are 4.8 × 10^{-10} and 0.7 × 10^{-10} cm^2, respectively [18]. These values produce the greatest OCT contrast enhancement (about 10^{-8} dB per colloidal GNS) [18] and accordingly the GNSs are, in principle, the most suitable contrast agent for cardiovascular OCT imaging. In aqueous solutions, these nanoparticles display a hydrodynamic diameter of 295 nm and a zeta potential of −24.5 mV. GNSs used in this work showed outstanding colloidal properties in both water and PBS, without signs of precipitation for months.

2.3 Cell lines, incubation conditions, and toxicity studies

Two different cell lines were investigated, i.e., HeLa cells and Jurkat cells. HeLa cells are an immortal cell line derived from human cervical cancer cells, with an epithelial phenotype. These cells divide an unlimited number of times *in vitro* under minimal survival conditions; accordingly, they are commonly used for cancer research [25]. In addition, as is typical for cancer cells, they are able to take up nanoparticles by passive targeting, usually by endocytosis. HeLa cells (ATCC CCL-2) were grown in Dulbecco's modified Eagle's medium with 10% fetal bovine serum (FBS). Jurkat cells (ATCC TIB 152) are an immortalized line of human T lymphocytes. They were grown in RPMI 1640 medium with 10% FBS. Both cell lines were cultured at 37 °C under 5% CO_2 and 95% humidity. Cells in exponential growth were used throughout all experiments. Incubation experiments were performed at 37 °C for 24 h using culture medium containing various concentrations of GNSs (0.05, 0.1, 0.5, 2.5, and 5 μg/mL). After incubation, cells were washed several times with PBS to remove excess GNSs that did not adhere or were not internalized by the cells. After incubation with GNSs, HeLa cells were trypsinized. The detached cells were resuspended in PBS and centrifuged at 1,000 rpm at 4 °C for 5 min. This step was repeated three times to eliminate excess NPs. Jurkat cells were resuspended without trypsinization in PBS and subjected to three cycles of centrifugation in order to eliminate excess GNSs.

Then, the incubated cell/PBS solutions were injected in a tube containing the OCT clinical catheter (see Fig. 1(a)) for optical imaging.

The viability of HeLa cells exposed to GNSs was analyzed by the 3-[4,5-dimethylthiazol-2-yl]-2,5-diphenyltetrazoliumbromide (MTT) colorimetric assay [26], a method based on the activity of mitochondrial dehydrogenases to reduce the tetrazolium salt MTT, yielding a violet-colored and insoluble compound, formazan. HeLa cells were incubated for 24 h with GNSs at various concentrations. After 24 h, the cells were incubated with MTT (0.5 ng/mL in Dulbecco's Modified Eagle's medium (DMEM) with 10% FBS) over 2–3 h at 37 °C. Then, the medium was removed and crystallized formazan was dissolved in dimethyl sulfoxide (DMSO). Immediately afterwards, absorbance at 542 nm was measured using a plate reader (Spectra Fluor 4; TECAN, Männedorf, Switzerland). Cell viability was estimated as a percentage relative to the mean absorption obtained from control cells (not incubated with the GNSs; 100% viability).

2.4 Dark-field microscopy

DFM was employed to prove the incorporation of GNSs in cells; this is a good technique to localize and monitor plasmonic nanoparticles *in vitro* [27]. DFM experiments were performed using both HeLa and Jurkat cells that were fixed after concentration with PBS solutions containing different dilutions of GNSs. Images were obtained using a microscope equipped with a dark-field condenser with a numerical aperture of 0.80–0.95. A 20× microscope objective with a numerical aperture of 0.4 was used. Illumination was performed employing a broadband white source. Under these experimental conditions, GNSs appear in dark-field images as bright red spots. Incubation efficiency was derived by computing the number of these spots inside individual cells.

2.5 Transmission electron microscopy

Transmission electron microscopy (TEM) was used to confirm that GNSs were intracellularly incorporated after 24 h of incubation described above. The JEOL JEM1010 (Tokyo, Japan) at an acceleration voltage of 80 kV was used for TEM.

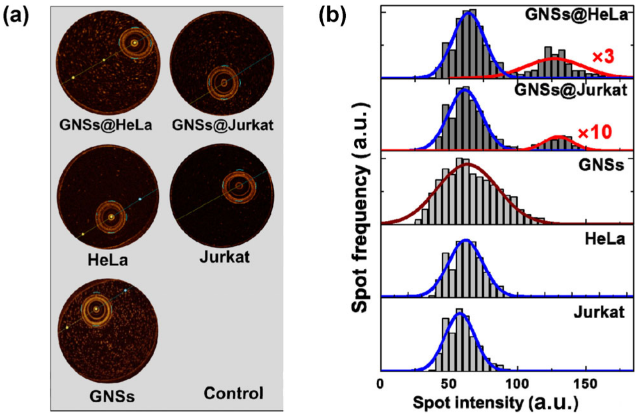

Figure 2 (a) CV-OCT cross-sectional images of GNSs suspended in PBS (2.5 μg/mL concentration), nonincubated HeLa and Jurkat cells in PBS, HeLa and Jurkat cells incubated for 24 h with a solution of GNSs in PBS. (b) Histograms of intensity, as calculated from the CV-OCT images are included in the left column. Note that free GNSs and free (nonincubated) Jurkat and HeLa cells yielded single Gaussian distributions centered at about 65 units (GNSs) and 60 units (free cells), whereas the incubation of HeLa and Jurkat cells with GNSs led to the appearance of high-intensity bands centered at about 120 units. The different fits to Gaussian distributions are shown as solid lines. ×3 and ×10 indicate the magnification.

3 Results and discussion

As indicated in the Introduction and with the purpose of studying CV-OCT contrast for living cells and its enhancement by passive incubation with GNSs, cytotoxicity was initially examined using various concentrations of GNSs by incubating HeLa cells for 24 h. The results of these experiments (Fig. S1 in the Electronic Supplementary Material (ESM)) indicated that for all concentrations (0.05, 0.1, 0.5, 2.5, and 5 mg/mL), cell viability was never less than 94% relative to the control.

Figure 2(a) shows OCT cross-sectional images of the tubing filled with only PBS, with a PBS solution containing GNS at 2.5 μg/mL, with PBS solutions containing nonincubated HeLa and Jurkat cells, and, finally, with a PBS solution containing HeLa and Jurkat cells after incubation with GNSs (24 h, 5 μg/mL). According to previous studies [18], different bright spots in cross-sectional images result from the backscattering of the 1,320 nm laser light produced by individual GNSs, individual cells, and/or individual cells containing GNSs. The right panel of Fig. 2 shows the spot intensity distribution (spot frequency as a function of the OCT spot intensity) obtained after an intensity analysis of the cross-sectional CV-OCT images. Each distribution was obtained by analyzing the intensity of 120 images obtained along the tube. The experiment was repeated at least 6 times for each concentration. For the solution containing only GNSs, a distribution of spot intensities was observed around a central spot intensity of about 65 (in the contrast units given by the CV-OCT software, hereafter u_{arb}) with a full width at half maximum (FWHM) of 50 u_{arb}. This distribution resembled a Gaussian distribution, as depicted by the best-fit curve displayed over the distribution. Cross-sectional images of the PBS solutions containing HeLa and Jurkat cells had bright OCT spots, demonstrating the ability of CV-OCT to detect individual cells. The corresponding spot diagrams are shown in the right panel of Fig. 2. In both cases, Gaussian distributions with peaks at about 59 u_{arb} and an FWHM close to 26 u_{arb} were obtained. Thus, when compared to the histogram of CV-OCT signal intensities provided by colloidal GNSs, it was clear that suspended cells (either HeLa or Jurkat) produce a much narrower distribution, peaking at slightly different OCT intensities. The right panel in Fig. 2 also includes the intensity histograms corresponding to the CV-OCT cross-sectional images obtained for cells that were incubated with GNSs (2.5 μg/mL) for 24 h. We clearly observed that the incubation process results in the appearance of a number of OCT spots at higher intensities than those obtained for single GNSs and for nonincubated cells. In these cases, the intensity histogram can be effectively described by the superposition of two Gaussian distributions as follows: 1) The dominant contribution corresponds to a Gaussian distribution centered at 62 u_{arb} with an FWHM close to 25 u_{arb}. Both characteristics are very similar to those obtained for the intensity histograms of nonincubated cells. Thus, we conclude that this contribution is associated with the sub-population of cells that did not incorporate GNSs during the incubation procedure. 2) The experimental data reveal an additional Gaussian distribution with a peak at about 125 u_{arb} and an FWHM of 50 u_{arb} for both HeLa and Jurkat cells. This second Gaussian distribution is associated with cells that internalized GNSs or adherent cells during the incubation procedure. Note that in these cases, the backscattering signal is expected to be higher, since it represents two different contributions, i.e., the backscattered signals produced by the medium-cell interface and by intracellular GNSs.

At this point, it should also be noted that, in accordance with the efficient washing procedures performed after incubation (described in the methodology section), no OCT signal was observed for free GNSs. The deconvolution of intensity histograms did not indicate any Gaussian band centered at around 65 u_{arb} with an FWHM of 50 u_{arb}, which is, as shown in Fig. 2, the signature of free GNSs in intensity histograms. Thus, the results presented in Fig. 2 clearly indicate that the incubation process gives rise to a population of cells with internalized GNSs together with free cells, i.e., cells that have not taken up GNSs. Intracellular incorporation of GNSs was also confirmed by DFM and TEM, as shown in Fig. 3. Figures 3(a) and 3(c) show, as relevant examples, images of HeLa and Jurkat cells obtained by DFM after 24 h of incubation with a PBS solution with GNSs at 2.5 μg/mL. According to previous studies [20, 28–30], the red spots observed in the DFM images are associated with individual GNSs. Thus, DFM images provide solid evidence for the incorporation of GNSs in both HeLa and Jurkat cells. This conclusion is further supported by TEM experiments. Figure 3(b) shows a representative TEM image of a HeLa cell section obtained after incubation, clearly showing the presence of GNSs in the cytoplasm.

Data summarized in Figs. 2 and 3 clearly demonstrate how the incubation of cells with GNSs leads to complex cross-sectional OCT images. These images consist of a collection of the brightest spots, whose distribution gives the population of successfully incubated cells, together with less intense spots, giving distributions related to free (nonincubated) cells. Therefore, the deconvolution of CV-OCT intensity histograms can be used to determine, in a qualitative way, the fraction of cells that have efficiently incorporated GNSs. This enables, for instance, investigations of how the concentration of GNSs in the cell culture medium during the incubation procedure affects the internalization efficiency. For this purpose, we analyzed the CV-OCT cross-sectional images of cells incubated for 24 h with solutions of PBS and GNSs at various concentrations (from 0.05 to 5 μg/mL). Figure 4(a) shows the cross-sectional images obtained for HeLa cells incubated with various concentrations of GNSs. The CV-OCT image obtained for nonincubated HeLa cells (control image) is also shown for comparison. In Fig. 4(b), the spot intensity distributions obtained for different incubation concentrations are displayed. As we were only interested in the signal generated by cells that efficiently incorporated GNSs, the intensity histograms included in Fig. 4 were restricted to the 120–180 u_{arb} range. Considering solely spot intensities in this range is equivalent to discriminating the signal

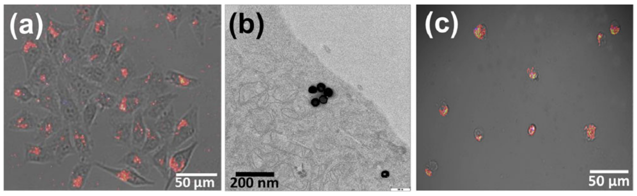

Figure 3 (a) Combined dark-field microscopy image and bright field microscopy image of HeLa cells incubated in a solution of GNSs in PBS at 2.5 μg/mL. (b) TEM image of a HeLa cells incubated in a solution of GNSs in PBS at 2.5 μg/mL in which the intracellular incorporation of GNSs was detected. (c) Combined dark-field microscopy image and bright-field microscopy image of Jurkat cells incubated in a solution of GNSs in PBS at 2.5 μg/mL. Incubation time was set to 24 h.

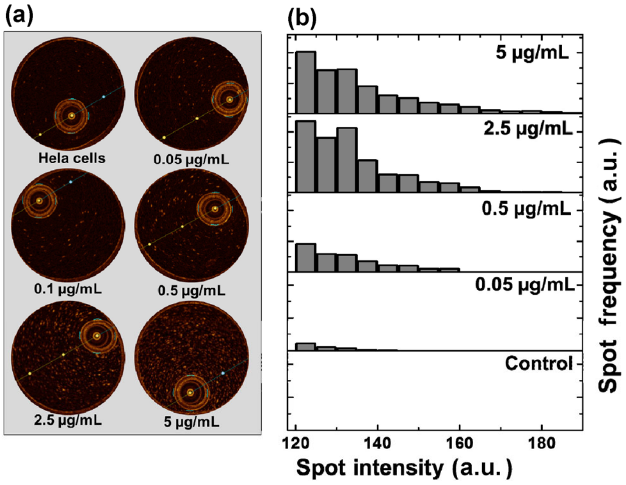

Figure 4 (a) CV-OCT cross-sectional images of nonincubated HeLa cells and HeLa cells incubated for 24 h with various concentrations of GNSs. (b) Intensity histograms as calculated from the CV-OCT cross-sectional images for spots intensities larger than 120 units (associated only with signals generated by HeLa cells that have incorporated GNSs).

generated by cells with efficient incorporation of GNSs from that generated by cells in which no GNS internalization took place. By direct computation of the total number of spots with intensities in the 120–180 u_{arb} range, it is therefore possible to obtain a relative measure of the population of cells with GNSs in their cytoplasm. Results obtained from the analysis of the intensity histograms in Fig. 4 are included in Fig. 5. These figures demonstrate that the subpopulation of HeLa cells that internalized GNSs increased as the concentration of GNSs increased in the culture medium. CV-OCT images revealed that for GNS concentrations below 0.5 μg/mL the internalization efficiency strongly depends on the GNS concentration, whereas for larger concentrations, the internalization efficiency becomes saturated and is only slightly dependent on the incubation concentration. A similar trend was observed when the adhesion efficiency of GNSs by Jurkat cells was determined based on CV-OCT images, as shown in Fig. 5. The CV-OCT images of Jurkat cells incubated with various concentrations of GNSs are shown in Fig. S2 in the ESM, together with TEM images (Fig. S3 in the ESM). In the case of Jurkat cells, interestingly, because of the lower phagocytosis ability of this cell line than that of HeLa cells, the GNSs appear to be attached to the membrane; nevertheless, the adhesion to the membrane was sufficient to increase the OCT signal, enabling the discrimination between individual cells and cells with GNSs. A comparison of data obtained by CV-OCT and those obtained by DFM could therefore be performed. We systematically studied the DFM images obtained for both HeLa and Jurkat cells incubated with various GNS concentrations (see representative examples in the upper panel of Fig. 5). These images clearly indicate that the number of red spots (related to individual GNSs) increases with the concentration of GNSs in the incubation medium. Analysis of DFM images also allows for a qualitative evaluation of the adhesion efficiency of GNSs by computing the average number of "red spots" per cell as a function of the GNS concentration. The concentration-dependent incubation efficiencies, as determined by DFM, for both HeLa and Jurkat cells are also shown in Fig. 5. It is clear that the DFM results were consistent with the CV-OCT results. The DFM images also reveal that the incorporation or adhesion efficiency of GNSs in living cells increases monotonically as the concentration of the GNSs in the culture medium increases. The DFM data also revealed a tendency towards saturation for concentrations larger than 0.5 μg/mL in very good agreement with the data extracted from CV-OCT images. This saturation behavior evidenced by both DFM and CV-OCT was in accordance with previous studies showing that the cellular uptake efficiency displays saturation behavior as the concentration of nanoparticles increases [31].

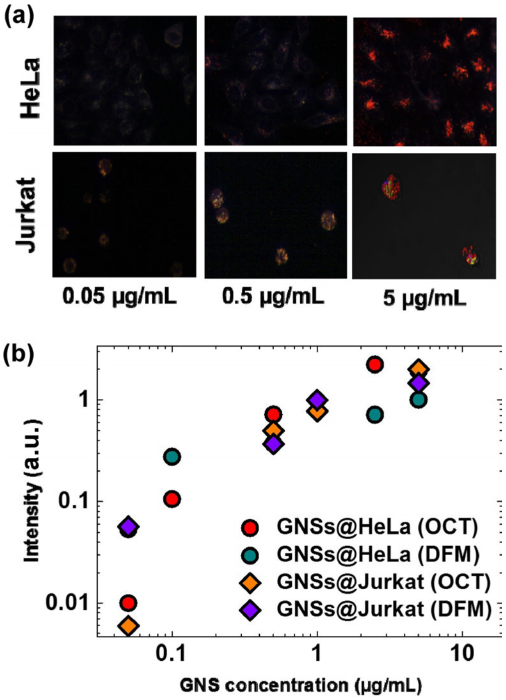

Figure 5 (a) Representative dark-field microscopy images of HeLa and Jurkat cells incubated with various concentrations of GNSs. Incubation time in all cases was 24 h. (b) Dark-field and OCT intensities generated from HeLa and Jurkat cells incubated with various concentrations of GNSs for a fixed time of 24 h. The OCT signal was calculated by integrating the frequency distribution signals for spot intensities above a threshold intensity of 120 (CV-OCT signal of successfully incubated cells). Symbols represent experimental data and the line is provided as a guide for visualization.

Finally, it should be noted that the unequivocal relation between OCT spots with intensities larger than 120 u_{arb} and GNS internalization allows not only detailed studies of the incubation efficiency, but also the three-dimensional localization of cells with GNSs in their cytoplasm. An example of this imaging capacity is given in Fig. 6. In Fig. 6(a), the raw CV-OCT image

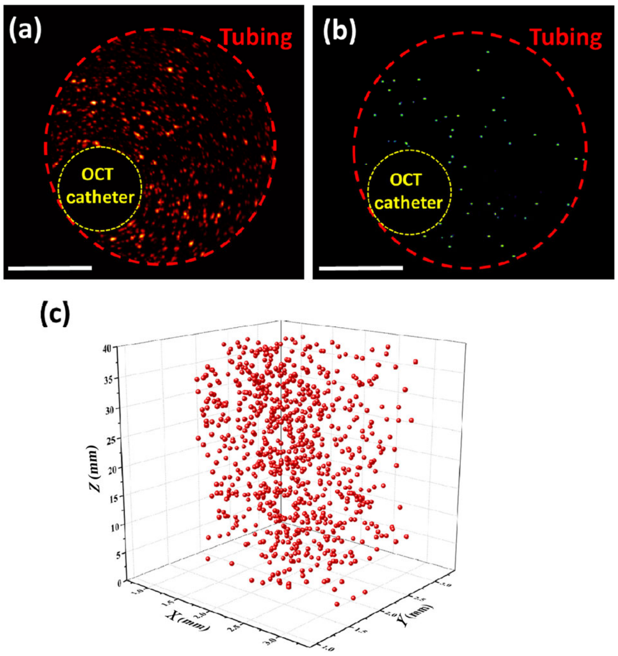

Figure 6 (a) Raw cross-sectional CV-OCT image of a suspension of HeLa cells after incubation with GNSs for 24 h. The concentration of GNSs in the culture medium during incubation was 2.5 μg/mL. (b) CV-OCT cross-sectional image of the same cell suspension used in (a), but after applying a threshold filtering to the raw image. The intensity threshold was set to 120 u_{arb} so that observed spots correspond to HeLa cells that internalized GNSs. (c) Three-dimensional CV-OCT image of the suspended HeLa cells that internalized GNSs. Each pixel providing a CV-OCT signal larger than 120 u_{arb} was identified as a single HeLa cell with internalized GNSs. Scale bar represents 1 mm.

of a suspension of HeLa cells after incubation for 24 h in a solution with PBS and GNSs at 2.5 μg/mL is shown. The CV-OCT raw image shows a large density of spots with a wide variety of intensities ranging from 40 to 180 u_{arb}. As discussed above, these spots reveal a high density of suspended HeLa cells. In order to isolate and obtain images of only HeLa cells that internalized GNSs efficiently, the raw CV-OCT images were modified by applying a filter with a single threshold level. Figure 6(b) shows the CV-OCT image corresponding to the data shown in Fig. 6(a) after removing the OCT spots with individual intensities below 120 u_{arb}. Since OCT intensities above 120 u_{arb} are only generated by HeLa cells with internalized GNSs, Fig. 6(b) corresponds, indeed, to an image of the sub-population of HeLa cells with GNSs. As explained in Section 2.1, the clinical CV-OCT system could also be used for three-dimensional imaging by pulling back the catheter. This possibility, together with the threshold level filtering, was exploited to obtain a three-dimensional image of the sub-population of HeLa cells with internalized GNSs. A representative example is given in Fig. 6(c). This last hypothesis suggests the possibility of real-time, three-dimensional tracking of living cells in the cardiovascular system by employing specifically targeted GNSs.

The application of GNSs in combination with a cardiovascular OCT system for cell imaging in an aqueous environment was demonstrated. As mentioned above, many clinical applications also require contrast enhancement within tissues. In order to demonstrate the potential application of GNSs to enhance the OCT contrast inside a tissue, a final experiment was designed in which the cardiovascular OCT catheter was positioned inside a breast tissue (*Gallus gallus domesticus*). Then, two injections (0.5 mL per injection) of an aqueous solution of GNSs (50 μg/mL) were performed in the proximity of the OCT catheter (see Fig. 7(a)). The cross-sectional images of the breast tissue obtained before and after the injection of

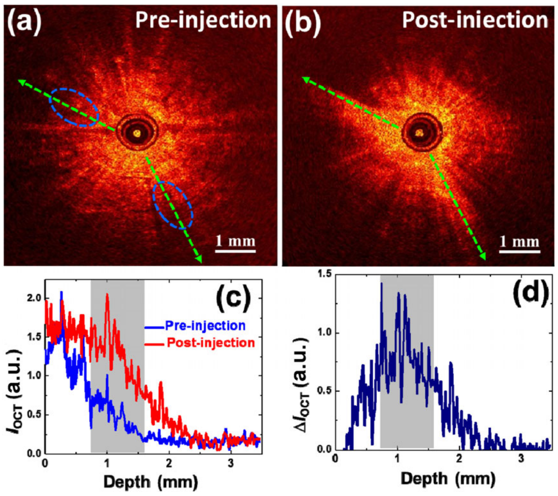

Figure 7 (a) Cross-sectional OCT image of a tissue prior to the injection of GNSs. An aqueous solution of GNSs (0.5 mL; 50 μg/mL) was injected in the areas delimited by the blue dashed lines. (b) Cross-sectional OCT image of the same tissue shown in (a) after the injection of an aqueous solution of GNSs. (c) OCT intensity (I_{OCT}) versus depth in the tissue, as obtained along the scan lines, is indicated by the green arrows in (a) and (b). (d) Difference between the OCT intensity obtained prior to and after the injection of GNSs (ΔI_{OCT}) as a function of the penetration depth in the tissue. The spatial extension of the GNSs within the tissue is indicated by the gray areas included in (c) and (d).

GNSs are shown in Figs. 7(a) and 7(b). A detailed comparison of these figures reveals a significant contrast enhancement at the injection locations. Figure 7(c) includes the average OCT intensity (I_{OCT}) against depth profiles obtained along the scan direction represented by the green arrows in Figs. 7(a) and 7(b), i.e., along two scan directions crossing the GNS injection areas. Figure 7(c) clearly demonstrates that the presence of GNSs leads to an OCT contrast enhancement between 0.8 and 1.6 mm, in good agreement with the location of the injected GNSs. This result is also observed when the OCT depth profile obtained prior to the injection is subtracted from the profile obtained after injection (ΔI_{OCT}). Figure 7(d) shows the relevant enhancement in the OCT contrast produced by the GNSs inside the tissue. Thus, the data included in Fig. 7 clearly demonstrate the potential use of GNSs as contrast agents for OCT imaging of tissues using cardiovascular clinical systems.

4 Conclusions

In summary, this work demonstrates that clinical CV-OCT allows the detection of individual cells suspended in biological fluids. The experimental results indicated that the backscattering contrast of individual cells could be substantially enhanced by the intracellular incorporation of specifically designed GNSs with high scattering cross-sections at the CV-OCT operating wavelength (1,320 nm). A simple intensity analysis of CV-OCT images enabled the identification and discrimination of different sub-populations within a suspension of living cells. In particular, a simple analysis of the intensity histograms for CV-OCT images allowed the detection of living cells for which GNS attachment occurred and made it possible to estimate the attachment efficiency and its relationship to the concentration of GNSs in the culture medium. These results were in excellent agreement with those obtained using alternative techniques, such as DFM and TEM.

As GNSs are easy to functionalize with biomolecules to target specific cell sites, the results of this study provide a new avenue for reliable molecular imaging by CV-OCT and thus could constitute the first step towards the development of new diagnostic procedures at the clinical level.

Acknowledgements

This work is supported by the Spanish Ministry of Economy and Competitiveness under Project No. MAT2016-75362-C3-1-R and by Instituto de Salud Carlos III under Project No. PI16/00812. J. H. acknowledges the scholarship from the China Scholarship Council (No. 201506650003). D. H. O. is grateful to the Spanish Ministry of Economy and Competitiveness for a Juan de la Cierva scholarship (No. FJCI-2014-21101).

Electronic Supplementary Material: Supplementary material (including further details of the experimental procedures, cell viability results, additional OCTand TEM images for the Jurkat cells) is available in the online version of this article at https://doi.org/10.1007/s12274-017-1674-4.

References

[1] Fercher, A. F.; Drexler, W.; Hitzenberger, C. K.; Lasser, T. Optical coherence tomography-principles and applications. *Rep. Prog. Phys.* **2003**, *66*, 239–303.

[2] Alfonso, F.; Sandoval, J.; Cárdenas, A.; Medina, M.; Cuevas, C.; Gonzalo, N. Optical coherence tomography: From research to clinical application. *Minerva Med.* **2012**, *103*, 441–464.

[3] Ashok, P. C.; Praveen, B. B.; Bellini, N.; Riches, A.; Dholakia, K.; Herrington, C. S. Multi-modal approach using Raman spectroscopy and optical coherence tomography for the discrimination of colonic adenocarcinoma from normal colon. *Biomed. Opt. Express* **2013**, *4*, 2179–2186.

[4] Fujimoto, J. G. Optical coherence tomography for ultrahigh resolution *in vivo* imaging. *Nat. Biotechnol.* **2003**, *21*, 1361–1367.

[5] Mattison, S. P.; Kim, W.; Park, J.; Applegate, B. E. Molecular imaging in optical coherence tomography. *Curr. Mol. Imaging* **2014**, *3*, 88–105.

[6] Zysk, A. M.; Nguyen, F. T.; Oldenburg, A. L.; Marks, D. L.; Boppart, S. A. Optical coherence tomography: A review of clinical development from bench to bedside. *J. Biomed. Opt.* **2007**, *12*, 051403.

[7] Bouma, B. E.; Yun, S.-H.; Vakoc, B. J.; Suter, M. J.; Tearney, G. J. Fourier-domain optical coherence tomography: Recent advances toward clinical utility. *Curr. Opin. Biotechnol.* **2009**, *20*, 111–118.

[8] Kennedy, B. F.; Kennedy, K. M.; Oldenburg, A. L.; Adie,

S. G.; Boppart, S. A.; Sampson, D. D. Optical coherence elastography. In *Optical Coherence Tomography: Technology and Applications*. Drexler, W.; Fujimoto, J. G., Eds.; Springer International Publishing: Switzerland, 2015; pp1007–1054.

[9] Alfonso, F.; Dutary, J.; Paulo, M.; Gonzalo, N.; Pérez-Vizcayno, M. J.; Jiménez-Quevedo, P.; Escaned, J.; Bañuelos, C.; Hernández, R.; Macaya, C. Combined use of optical coherence tomography and intravascular ultrasound imaging in patients undergoing coronary interventions for stent thrombosis. *Heart* **2012**, *98*, 1213–1220.

[10] Bezerra, H. G.; Costa, M. A.; Guagliumi, G.; Rollins, A. M.; Simon, D. I. Intracoronary optical coherence tomography: A comprehensive review: Clinical and research applications. *JACC*: *Cardiovasc*. *Interv*. **2009**, *2*, 1035–1046.

[11] Prati, F.; Stazi, F.; Dutary, J.; La Manna, A.; Di Giorgio, A.; Pawlosky, T.; Gonzalo, N.; Di Salvo, M. E.; Imola, F.; Tamburino, C. et al. Detection of very early stent healing after primary angioplasty: An optical coherence tomographic observational study of chromium cobaltum and first-generation drug-eluting stents. The detective study. *Heart* **2011**, *97*, 1841–1846.

[12] Rivero, F.; Bastante, T.; Cuesta, J.; Benedicto, A.; Restrepo, J. A.; Alfonso, F. Treatment of in-stent restenosis with bioresorbable vascular scaffolds: Optical coherence tomography insights. *Can*. *J*. *Cardiol*. **2015**, *31*, 255–259.

[13] Douma, K.; Prinzen, L.; Slaaf, D. W.; Reutelingsperger, C. P. M.; Biessen, E. A. L.; Hackeng, T. M.; Post, M. J.; van Zandvoort, M. A. M. J. Nanoparticles for optical molecular imaging of atherosclerosis. *Small* **2009**, *5*, 544–557.

[14] Chen, J. Y.; Saeki, F.; Wiley, B. J.; Cang, H.; Cobb, M. J.; Li, Z.-Y.; Au, L.; Zhang, H.; Kimmey, M. B.; Li, X. D. et al. Gold nanocages: Bioconjugation and their potential use as optical imaging contrast agents. *Nano Lett*. **2005**, *5*, 473–477.

[15] Bibikova, O.; Popov, A.; Bykov, A.; Prilepskii, A.; Kinnunen, M.; Kordas, K.; Bogatyrev, V.; Khlebtsov, N.; Vainio, S.; Tuchin, V. Optical properties of plasmon-resonant bare and silica-coated nanostars used for cell imaging. *J*. *Biomed*. *Opt*. **2015**, *20*, 076017.

[16] Skrabalak, S. E.; Chen, J.; Au, L.; Lu, X.; Li, X.; Xia, Y. Gold nanocages for biomedical applications. *Adv*. *Mater*. **2007**, *19*, 3177–3184.

[17] Gobin, A. M.; Lee, M. H.; Halas, N. J.; James, W. D.; Drezek, R. A.; West, J. L. Near-infrared resonant nanoshells for combined optical imaging and photothermal cancer therapy. *Nano Lett*. **2007**, *7*, 1929–1934.

[18] Hu, J.; Rivero, F.; Torres, R. A.; Ramírez, H. L.; Rodríguez, E. M.; Alfonso, F.; Solé, J. G.; Jaque, D. Dynamic single gold nanoparticle visualization by clinical intracoronary optical coherence tomography. *J*. *Biophotonics* **2017**, *10*, 674–682.

[19] Skala, M. C.; Crow, M. J.; Wax, A.; Izatt, J. A. Photothermal optical coherence tomography of epidermal growth factor receptor in live cells using immunotargeted gold nanospheres. *Nano Lett*. **2008**, *8*, 3461–3467.

[20] Loo, C.; Lowery, A.; Halas, N.; West, J.; Drezek, R. Immunotargeted nanoshells for integrated cancer imaging and therapy. *Nano Lett*. **2005**, *5*, 709–711.

[21] De León, Y. P.; Pichardo-Molina, J. L.; Ochoa, N. A.; Luna-Moreno, D. Contrast enhancement of optical coherence tomography images using branched gold nanoparticles. *J*. *Nanomater*. **2012**, *2012*, 571015.

[22] De La Zerda, A.; Prabhulkar, S.; Perez, V. L.; Ruggeri, M.; Paranjape, A. S.; Habte, F.; Gambhir, S. S.; Awdeh, R. M. Optical coherence contrast imaging using gold nanorods in living mice eyes. *Clin*. *Exp*. *Ophthalmol*. **2015**, *43*, 358–366.

[23] Adler, D. C.; Huang, S.-W.; Huber, R.; Fujimoto, J. G. Photothermal detection of gold nanoparticles using phase-sensitive optical coherence tomography. *Opt*. *Express* **2008**, *16*, 4376–4393.

[24] Fratoddi, I.; Venditti, I.; Cametti, C.; Russo, M. V. How toxic are gold nanoparticles? The state-of-the-art. *Nano Res*. **2015**, *8*, 1771–1799.

[25] Masters, J. R. HeLa cells 50 years on: The good, the bad and the ugly. *Nat*. *Rev*. *Cancer* **2002**, *2*, 315–319.

[26] Mosmann, T. Rapid colorimetric assay for cellular growth and survival: Application to proliferation and cytotoxicity assays. *J*. *Immunol*. *Methods* **1983**, *65*, 55–63.

[27] Li, M.; Lohmüller, T.; Feldmann, J. Optical injection of gold nanoparticles into living cells. *Nano Lett*. **2015**, *15*, 770–775.

[28] Cui, Y.; Wang, X. L.; Ren, W.; Liu, J.; Irudayaraj, J. Optical clearing delivers ultrasensitive hyperspectral dark-field imaging for single-cell evaluation. *ACS Nano* **2016**, *10*, 3132–3143.

[29] Wax, A.; Sokolov, K. Molecular imaging and darkfield microspectroscopy of live cells using gold plasmonic nanoparticles. *Laser Photonics Rev*. **2009**, *3*, 146–158.

[30] Qian, W.; Huang, X. H.; Kang, B.; El-Sayed, M. A. Dark-field light scattering imaging of living cancer cell component from birth through division using bioconjugated gold nanoprobes. *J*. *Biomed*. *Opt*. **2010**, *15*, 046025.

[31] Jaque, D.; Maestro, L. M.; del Rosal, B.; Haro-Gonzalez, P.; Benayas, A.; Plaza, J. L.; Rodríguez, E. M.; Solé, J. G. Nanoparticles for photothermal therapies. *Nanoscale* **2014**, *6*, 9494–9530.